European Conference on Computational Fluid Dynamics
ECCOMAS CFD 2006
P. Wesseling, E. Oñate and J. Périaux (Eds)


# LES AND URANS UNSTEADY BOUNDARY LAYER STRATEGIES FOR PULSATING AND OSCILLATING TURBULENT CHANNEL FLOW APPLICATIONS.

**Daniele Panara*, Mauro Porta† and Thilo Schoenfeld†**

*DLR, Deutsches Zentrum für Luft- und Raumfahrt e. V.
Institut für Verbrennungstechnik
Pfaffenwaldring 38-40, 70569 Stuttgart
e-mail: daniele.panara@dlr.de
web page: http://www.dlr.de/vt

†CERFACS, Centre Europeen de Recherche et de Formation Avancee en Calcul Scientifique,
Avenue Gaspard Coriolis 42. 31057 Toulouse Cedex 01. France.
e-mail: mauro.porta@cerfacs.fr

**Key words:** Fluid Dynamics, Turbulence, URANS, LES, Pulsating Flow, Oscillating Flow, Near Wall Modeling, Wall Shear Stress.

**Abstract.** *The use of wall functions has been investigated for LES and URANS numerical simulation in pulsating and oscillating channel flow applications. The results show that the wall function approach is accurate in the so-called quasi-steady regime but there are discrepancies with the experimental results in the intermediate frequency range. A special attention is given to the wall-shear stress prediction, and in particular on the wall-shear stress phase shift with respect to the free stream velocity. In order to capture such unsteady flow effects, the boundary layer needs to be resolved. Different approaches such as Low Reynolds Number near wall turbulence modeling (URANS) or the proposed Wall-Normal Resolved strategy (LES) seem to be suited for this purpose. The drawback is unfortunately the increasing of computational points in the boundary layer and consequently the higher computational costs.*

## 1 INTRODUCTION

With the continuous growing of the computational resources, the use of unsteady numerical simulations is becoming a strategic tool in designing complex industrial components. Many examples of that can be found in turbomachinery and combustion chamber applications. Commercial CFD softwares are widely used in industry and a critical factor for the design development resides in an optimal balance between numerical costs and prediction accuracy. Unsteady Reynolds averaged Navier-Stokes (URANS) and, in the last years, Large Eddy Simulations (LES) have been used increasingly by industry for the study of critical components. For internal turbulent flow simulations, in order to save

computational time, the wall-boundary layer resolution is often neglected. In both, the LES and URANS approach, the tendency is to model the inner-part of the boundary layer by means of so-called wall functions. The use of wall functions significantly reduces the number of computational points required in the boundary layer region and for this reason it is widely used. However, it is questionable whether in pulsating and unsteady flow conditions the hypothesis under which the wall functions have been developed are still valid. A deeper investigation on the accuracy of the use of wall functions for unsteady turbulent flow applications is therefore needed.

Despite their simple geometry, pulsating channel flows are representative of many interesting industrial configurations. In the present work, the accuracy of the use of wall functions in LES and URANS is investigated by means of such testing cases. Our attention is focused on the unsteady wall-shear stress prediction since it is important also as an indirect measure of the unsteady wall heat transfer.

In the present work two very different CFD research solvers are used. OpenFoam[1] has been chosen for the URANS calculations and AVBP[2] for the LES calculations. These two codes differ not only for the discretisation schemes used but also for the mathematical formulation of the problem. A brief description of the codes and governing equations will be given in the next sections. For the near wall treatment, both codes employ a similar wall function approach. Details about the LES code and its wall functions implementation are given in section (2) and (2.1). In section (2.2) a validation of the LES code in an oscillating channel flow configuration against DNS (Direct Numerical Simulation) results from Spalart and Baldwin[3] is presented. Details of the URANS solver are given in section (3) and the implementation of wall functions is briefly described in section (3.1). The URANS code is validated against the experimental results of Tardu et al.[4] in section (3.2). Finally in the last part of the paper, the URANS results obtained in section (3.2) for pulsating flow conditions are compared with comparable LES pulsating channel simulations and experimental results using characteristic non-dimensional parameters. Main attention is paid on wall-shear stress and its phase shift respect to the free stream velocity.

## 2 LES Solver

DNS and LES computations, object of this work, were performed using the AVBP code developed by CERFACS and IFP. AVBP is a parallel CFD code that solves the laminar and turbulent compressible Navier-Stokes equations in two and three space dimensions on unstructured and hybrid grids. The data structure of AVBP employs a cell-vertex finite-volume approximation. The basic numerical methods are based on a Lax-Wendroff or a Finite-Element type low-dissipation Taylor-Galerkin discretisation in combination with a linear-preserving artificial viscosity model. In this paper only the former was used, the study of the influence of the numerical scheme on the solution remains open for future works. The time discretisation is explicit making use of a Runge-Kutta multi-stage time stepping. For turbulent compressible flows, AVBP solves the LES formulation of the

Navier-Stokes equations. In the LES approach, the governing equation are filtered in space before discretising and solving. Additional unresolved terms appear in the convective fluxes. For the Reynolds stresses we have:

$$\overline{\tau_{ij}}^t = -\bar{\rho}(\widetilde{u_i u_j} - \tilde{u_i}\tilde{u_j}) \tag{1}$$

The over-bar represents a filtered numerically resolved quantity and the tilde represents a mass-weighted Favre filtering.

$\rho$ and $u_i$ represent respectively the density and the $i^{th}$ component of the velocity vector $u$. The unresolved sub-grid scale (SGS) terms are generally closed using the following formulation:

$$\overline{\tau_{ij}}^t = 2\bar{\rho}\nu_t\widetilde{S_{ij}} - \frac{1}{3}\overline{\tau_{ll}}^t\delta_{ij} \tag{2}$$

where

$$\widetilde{S_{ij}} = \frac{1}{2}(\frac{\partial\tilde{u_i}}{\partial x_j} + \frac{\partial\tilde{u_j}}{\partial x_i}) - \frac{1}{3}\frac{\partial\tilde{u_k}}{\partial x_k}\delta_{ij} \tag{3}$$

In our computations two different closure are used: the classical Smagorinsky model[5]

$$\nu_t = (C_S\Delta)^2\sqrt{2\widetilde{S_{ij}}\widetilde{S_{ij}}} \tag{4}$$

and the WALE model[6]

$$\nu_t = (C_w\Delta)^2\frac{(s_{ij}^d s_{ij}^d)^{3/2}}{(\widetilde{S_{ij}}\widetilde{S_{ij}})^{5/2} + (s_{ij}^d s_{ij}^d)^{5/4}} \tag{5}$$

where $C_w$ and $C_S$ are model constants ( $C_w = 0.4929$ and $C_S = 0.18$ ), $\Delta$ is the characteristic filter length and

$$s_{ij}^d = \frac{1}{2}(\tilde{g}_{ij}^2 + \tilde{g}_{ji}^2) - \frac{1}{3}\tilde{g}_{kk}^2\delta_{ij} \tag{6}$$

where $\tilde{g}_{ij}$ denotes the resolved velocity gradient. The WALE model was developed for wall bounded flows in an attempt to recover the scaling laws of the wall without using the wall function approach.

### 2.1 Wall Functions Implementation

The wall law implemented in AVBP is presented in detail by Schmitt[8] and is here shortly described. As mentioned above AVBP uses a cell-vertex scheme. All quantities are stored at the cell-corners. For the calculation of the viscous fluxes AVBP needs the shear stresses at the cell boundary and heat fluxes. Imposing the appropriate values of velocity and temperature at the boundary plus the correct fluxes, using the wall-law formulations, constrains the flow too much and leads to oscillatory solutions. The strategy used by

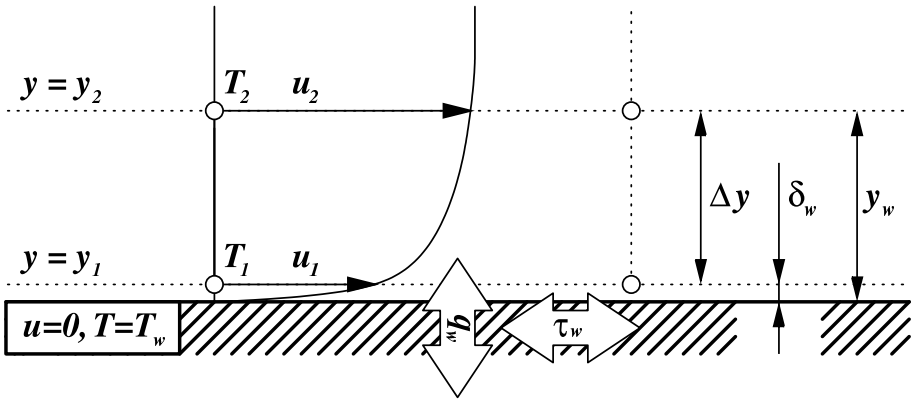


Figure 1: Typical velocity profile near the wall and notation used for near-wall quantities.

| | |
|---|---|
| Step 1 | Compute $u_\tau$ iteratively from Eq. (8) or (9) with $y^+ = \frac{\bar{u}_\tau y}{\nu}$ and $u^+ = \frac{\bar{u}}{\bar{u}_\tau}$ Input values: $\overline{u} = u_2, \nu = \nu(T_1), y = \Delta y$. |
| Step 2 | Compute $\tau_w$ from $\bar{u}_\tau = \sqrt{\frac{\bar{\tau}_w}{\bar{\rho}}}$ with $\rho = \rho_1$. |
| Step 3 | Apply $\tau_w$ and advance flow equations. |
| Step 4 | Set normal component of $u_1$ to zero and go to Step 1. |

Table 1: Working principle of the wall-function boundary condition.

Schmitt is then to impose the wall-shear stress $\tau_w$ (and heat flux $q_w$) at the boundary using the wall-function approach without fixing the value of velocity and temperature at the cell corners ($u_1$ and $T_1$ in Figure (1)). Only the normal component of the velocity at the wall is imposed to vanish for continuity reasons. This is equivalent, as shown in Figure (1), to imagine the real wall boundary shifted by a small distance $\delta_w$ away from the computational domain. Assuming that the shift is small compared to the distance between the wall and the first point in which the wall-function is evaluated ($\delta_w \ll y_w$), it can be neglected when computing the wall distance. The wall shear stress is then imposed at the boundary following the steps in Table (1).

### 2.2 LES code Validation for Oscillating Flow

In order to validate the code in a turbulent oscillating channel flow application the numerical results are compared with a DNS from Spalart and Baldwin[3]. Two series of near wall treatments have been employed: the Wall Function approach as explained in section (2.1) and a so-called Wall-Normal Resolved approach.

The computational domain consists of a cubic box of $0.006m$ side centered in the axis origin. On the upper and lower box-sides solid wall boundary conditions are applied. The other remaining boundaries are treated as periodic. The flow is considered aligned with the x axis. The y axis is normal to the walls and the z axis is aligned with the span-wise direction.

The flow is oscillated using a pressure source term which realizes an harmonic pressure gradient.

For the Wall-Function computations an equally-spaced 31x31x31 grid in the three axis direction is used. A wall function treatment is employed in the near wall region as explained in (2.1).

In the Wall-Normal Resolved computations, the used grid is equally spaced in the x and z directions, but stretched in the wall-normal direction in order to resolve the boundary layer up to a $y^+$ value of the order of 2. The $y^+$ value is computed using in first approximation the usual steady channel flow correlations and the maximum velocity value in the cycle. An hyperbolic tangent stretching law has been employed.

The fluid considered is $N_2$ with a kinematic viscosity value of $1.710^{-5}m^2/s$. The maximum $\tau_w$ is calculated considering the maximum cycle velocity at the channel center line. We choose a maximum velocity amplitude, $U_{max} \approx 70m/s$ and a frequency of $100Hz$ in order to have a Reynolds number based on the Stokes length around 1000 and comparable with the results in Spalart and Baldwin[3].

For the Wall-Resolved computations, the WALE model has been used in order to reproduce the asymptotic behavior of the SGS turbulence terms to the wall[6]. For the Wall-Function computations, the SGS viscous terms have been closed using the classical Smagorinsky model.

### 2.2.1 Results

The numerical results for the Wall-Function and Wall-Normal Resolved computations are reported in Figure from (4) to (8) and from (9) to (13). For each time phase ($\pi/6$, $\pi/3$, $2\pi/3$, $5\pi/6$ and $\pi$) the non-dimensional values of the wall shear stress ($\tau_w/U_o^2$), the velocity distribution ($u/U_o$), the fluctuation of the velocity components ($u'/U_o$,$v'/U_o$ and $w'/U_o$) and the dimensional pressure fluctuations ($P'$) are reported in function of the non-dimensional wall distance. The value of flow quantities have been non-dimensionalised using the velocity amplitude ($U_o$) and the Stokes length ($\delta_l$).

The results are obtained by phase-locking averaging the numerical instantaneous values over several cycles. As seen from the graphs, the velocity profiles are well captured by either near wall approach. We notice a non-zero value of the velocity at the wall due to the wall-function implementation as explained in section (2.1). In the Wall-Function computations, the values of the velocity fluctuations are not well captured at the wall since near the wall the turbulent structure are not resolved but indeed modeled by the wall law. The Wall-Normal Resolved computations instead, reproduce quite well the turbulent

structure at the wall even if the grid is resolved only in the y-direction. The values of $u'/U_o$,$v'/U_o$ and $w'/U_o$ agree very well with the DNS results. Concerning $\tau_w$ we observe a good agreement in both series of computations. We notice that the Wall-Normal Resolved computations predict pressure fluctuations one order of magnitude larger with respect to the Wall-Functions computations. In Figure (14) $\tau_w$ is reported vs. phase and compared with the DNS results. The Wall-Function computations seem to better reproduce the amplitude of the wall shear stress oscillations. We notice a little phase shift between the peak value of $\tau_w$ that is not present in the Wall-Normal Resolved results. The Wall-Normal Resolved $\tau_w$ predictions seem to underestimate the peak value of the wall-shear stress but seem to be more in phase with the DNS data. The overall behavior of both approaches is quite good for this oscillation frequency.

The most striking discrepancy is on the pressure fluctuation prediction. Unfortunately, no direct DNS data are available. In Figure (15) the pressure term of the Reynolds-stress budget is reported compared with the DNS data. Only the phase $\phi = \pi$ has been reported for shortness but similar results have been obtained in all the other phases. The figure shows that the Wall-Normal Resolved result agree with the DNS data. The Wall-Function results are not reported in the graph since out of scale. The results oscillations are probably due to numerical noise related to the discretisation scheme employed.

$$P_{term} = \Pi_{12} = -\frac{1}{\rho}\Big(\overline{u'\frac{\partial P'}{\partial y} - v'\frac{\partial P'}{\partial x}}\Big) \tag{7}$$

## 3 URANS Solver

The URANS calculation where performed using the OpenFoam solver. OpenFoam (Open Field Operation and Manipulation) is a CFD toolbox that uses finite volume numerics to solve systems of partial differential equations ascribed on any 3D unstructured mesh of polyhedral cells. The top-level code used for our computations is the standard OpenFoam solver turbFoam, a transient solver for incompressible, turbulent flow that will be shortly described below.

turbFoam solves the URANS equation for a turbulent fluid flow using a robust, implicit, pressure-velocity, iterative algorithm based on the PISO scheme[7] (Pressure-Implicit with Splitting of Operators).

For the URANS simulations, two series of near wall treatments have been employed: the Wall Function approach as explained in section (3.1) together with a $k$-$\epsilon$ High Reynolds Number model and a resolved boundary layer approach using the $k$-$\epsilon$ Low Reynolds Number model from Launder and Sharma[9].

### 3.1 Wall Functions Implementation

The use of wall functions is based on two important assumptions:

1. The validity of the universal law of the wall

$$u^+ = y^+ \qquad 0 < y^+ < 5 \tag{8}$$

$$u^+ = \frac{1}{\kappa} \ln y^+ + C \qquad y^+ > 40 \tag{9}$$

2. The assumption of turbulent local equilibrium in the near wall region:

$$\mathcal{P} = \epsilon; \quad \mathcal{P} = \nu_t (\tfrac{\partial u}{\partial y})^2 \tag{10}$$

where $\mathcal{P}$ and $\epsilon$ represent the production and dissipation term of the turbulent kinetic energy transport equation. The turbulent kinetic viscosity $\nu_t$ in the $k$-$\epsilon$ turbulent model formulation depends on the solution of the two additional transport equations for $k$ and $\epsilon$.

In the above hypothesis, assuming a known distribution of $k$ and $\epsilon$ near the wall by solving their transport equation, it is possible to obtain an expression for $\tau_w$ that can be used as boundary condition for the solution of the momentum equation.

### 3.2 URANS code Validation for Pulsating Flow

The URANS code is validated against the experimental data of Tardu et al.[4]. The test channel is 100 mm in width, 2600 mm in length and 1000 mm in span. The working fluid is water and the flow is pulsated using a special device which details are given in [4]. The flow can be considered isothermal. The flow pulsations at the channel center line can be expressed:

$$u_c(t) = U_c(1 + a_{\tilde{uc}} \cos \omega t) \tag{11}$$

or

$$u_c(t) = U_c + A_{\tilde{uc}} \cos \omega t \tag{12}$$

The values of $a_{\tilde{uc}}$ are varied in the experiment in the range from 0.1 to 0.6. The value of $U_c$ varies up to 0.5 $m/s$. The pulsation frequency is given in relation to the so called dimensionless viscous Stokes layer thickness ($l_s^+$) defined below

$$l_s^+ = \sqrt{\frac{2}{\omega^+}} \tag{13}$$

with

$$\omega^+ = \frac{\omega \nu}{\bar{u}_w^2} \tag{14}$$

Where $\bar{u}_w^2$ is the skin friction velocity of the relative steady channel case with $U_c$ velocity at the channel center line.

The grid employed with Low Reynolds Number turbulence models ( LR-Grid ) is a two dimensional grid with 150x80 points. The points in the direction normal to the channel wall are stretched using a simple grading algorithm in which the ratio between the larger and the smaller cell has been set to 5. The instantaneous values of $y^+$ are varying during the unsteady computations but are always between 10 and one.

The grid employed with wall functions ( HR-Grid ) is not stretched and it is composed of 150x40 points. As expected the Wall Functions approach requires a minor number of computational points and the $y^+$ values are in this case of the order of 50.

Concerning the boundary conditions, a turbulent inlet profile is pulsated at the inlet and a fixed static value of pressure is prescribed at the outlet.

### 3.2.1 Results

In Figure (2) we report the near-wall velocity profiles in different phases compared with the experimental results for $l_s^+ = 8.1$,$a_{\tilde{u}c} = 0.64$ and $U_c = 0.169\ m/s$. The computed skin friction velocity for the steady case is 0.92 $cm/s$. According to the definition of $l_s^+$ it is possible to calculate the pulsating flow frequency: $f = 0.41\ Hz$. The high Reynolds number and low Reynolds number boundary layer treatments are indicated with HR and LR. The figure shows a first limitation of the wall law approach. In this flow regime, the magnitude of the pulsations determines the flow reversal close to the solid walls. This is not captured by the HR model even though there is a quite good agreement between the HR and LR model far from the wall.

Computing the wall shear stress according to the wall-function formulation and using the following for the LR model:

$$\bar{\tau}_w = \bar{\rho}\nu \frac{\partial \bar{u}}{\partial y}\Big|_w \tag{15}$$

a phase shift with respect to the velocity centreline of $-8°$ and $33°$ as shown in Figure (3) has been obtained. Besides the calculations done for $l_s^+ = 8.1$, a variety of further simulations was done for other values of $l_s^+$. In Figure (3) the value of wall-shear stress phase shift is shown as function of the dimensionless viscous Stokes layer thickness $l_s^+$. The numerical results are compared with the experimental results reported by Tardu[4] (symbols in black). The graph shows the incapability of the wall law approach to predict the experimental wall-shear stress phase shift. The red and blue vertical lines separate the regimes of quasi-laminar and quasi-steady boundary layer behavior. Depending on the pulsation frequency, different boundary layer regimes are experienced. In the quasi-steady regime, the turbulence has time to relax to the local (in time) equilibrium. The flow can be studied as a succession of steady states and the wall function assumption seems to be still valid in this flow conditions as shown in Figure (3). With increasing frequency the turbulence production and dissipation start to show a phase lag. In this situation a

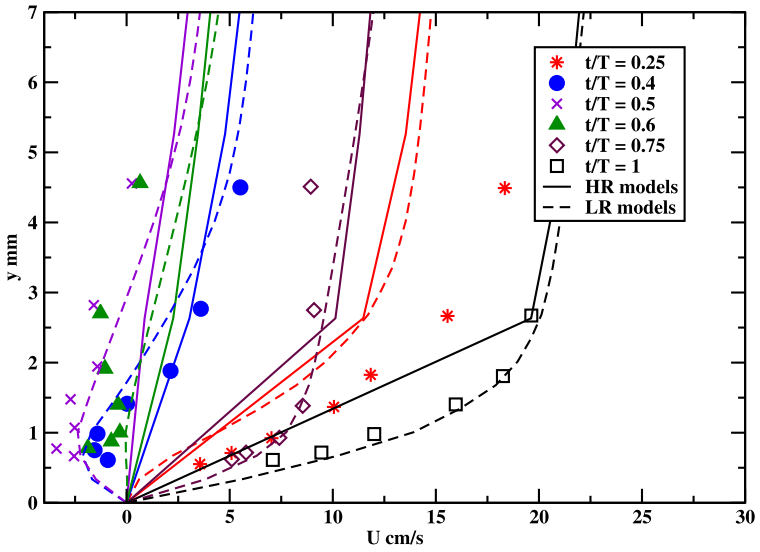


Figure 2: Instantaneous velocity profiles in the presence of reverse flow. $U_c = 16.9\ cm/s$, $a_{\tilde{uc}} = 0.64$, $l_s^+ = 8.1$.

change in amplitude and phase of the wall-shear stress in respect of the outer velocity is measured. A Stokes layer, where the effects of the outer flow oscillations are confined, occurs. The thickness of the Stokes Layer decreases with increasing forcing frequency and in the inertia dominated or ( quasi-laminar ) regime the Stokes layer resides completely within the viscous sub layer. In this case a flow solution can be obtained combining the laminar Stokes solution in the laminar sub-layer with a turbulent plug flow far from the wall.

## 4 LES and URANS Near Wall Numerical Predictions in Turbulent Pulsating Flows

For the comparison between URANS and LES near-wall numerical prediction in turbulent pulsating flow we designed a LES pulsating channel case in order to meet the value of $l_s^+$ considered by Tardu et al.[4]. The computational domain and boundary conditions are analogous to the validating oscillating case in section (2.2). The source term has been expressed as follows:

$$-\frac{1}{\rho}\frac{\partial P}{\partial x} = K_{osc}\sin\omega t + K \tag{16}$$

$K_{osc}$ in first approximation has been evaluated using the laminar analytical solution for oscillating flows ($K_{osc} = U_c\omega$). $K$ has been chosen, as a first approximation, to balance

the wall mean value shear-stress:

$$K = \frac{2\bar{\tau}_w}{h} \tag{17}$$

where $h$ is the channel heigth and in our case the size of the cubic numerical domain chosen. For the case of $l_s^+ = 14.14$ we considered a value of $U_c = 70\ m/s$ and an heigth of the channel $h = 0.006\ m$. We obtained then using steady channel correlation a value of $\bar{\tau}_w = 13.88\ N/m^2$ and $\bar{u}_\tau = 3.48\ m/s$ with a channel Reynolds number of 98800. The consequent pulsation frequency can be sought from the $l_s^+$ definition and it is around 1140 $Hz$.

The amplitude of the velocity pulsation ($A_{\tilde{uc}}$) has been chosen equal to 20 $m/s$. For different values of $l_s^+$ only the oscillating frequency has been changed in the evaluation of the source terms. All the computations are then made with the same channel size ($h = 0.006\ m$) and the computed values of $U_c$ and $A_{\tilde{uc}}$ are always around 70 and 20 $m/s$.

For the Wall-Function computation an equally spaced grid 31x31x11 has been used. For the Wall-Normal Resolved computations a wall-normal stretched grid 21x21x21 with an hyperbolic tangent stretching law has been employed. For comparison, a DNS channel of $h = 0.0015\ m$ with same values of $U_c$ and $A_{\tilde{uc}}$ has also been computed. In order to match the nominal condition of $l_s^+ = 14.14$ the pulsation frequency has been set to 1500 $Hz$. The DNS grid consists of a wall-normal stretched grid with 73x73x9 points.

The results are shown in Figure (3)

## 5 Conclusions

The use of wall-functions for LES and URANS has been investigated paying special attention to the wall shear stress phase shift. The LES computations were validated using the DNS results from Spalart and Baldwin[3] on oscillating flows showing a good agreement between the Wall-Function and Wall-Normal Resolved approaches. When the two near wall modeling were tested in pulsating conditions discrepancies have been found in the wall-shear stress phase shift predictions. Similar results have been obtained also for URANS calculations using as a test case the experimental results from Tardu et al.[4]. It is interesting at this stage to point out that the oscillations in the case of Spalart and Baldwin are well above the quasi-steady regime. The $l_s^+$ parameter in this case has been computed using the maximum skin friction velocity during the period of oscillation. We do not expect indeed strong phase shift effects in cases with large values of $l_s^+$ and for this reason the validation results are in accordance with our findings. The Wall-Normal Resolved computations and the Low-Reynolds turbulent model seem to capture the unsteady effects of pulsation on the wall-shear stress phase shift. The use of wall functions is accurate only in cases in which the oscillations are well above the quasi-steady regime. In all the other cases the use of wall-functions in URANS and LES computations is questionable especially in applications for which phase lags can play an important role such as the prediction of thermo-acoustic instabilities.

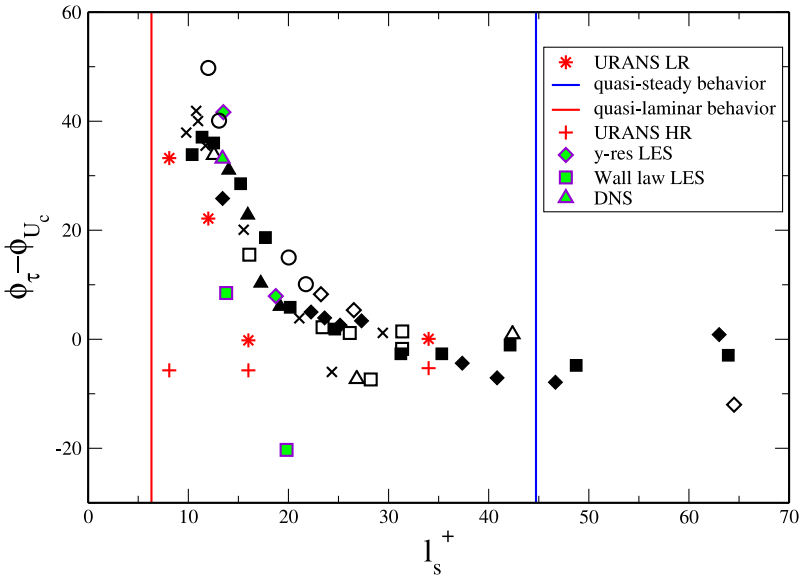


Figure 3: Wall shear stress phase shift dependence on pulsation frequency

## 6 Acknowledgements

This work was carried out within the Marie Curie Research Training Network FLUIST-COM ( Fluid-Structure Interaction for Combustion Systems ) under FP6, European Commission, DG XII.

## 7 Figures

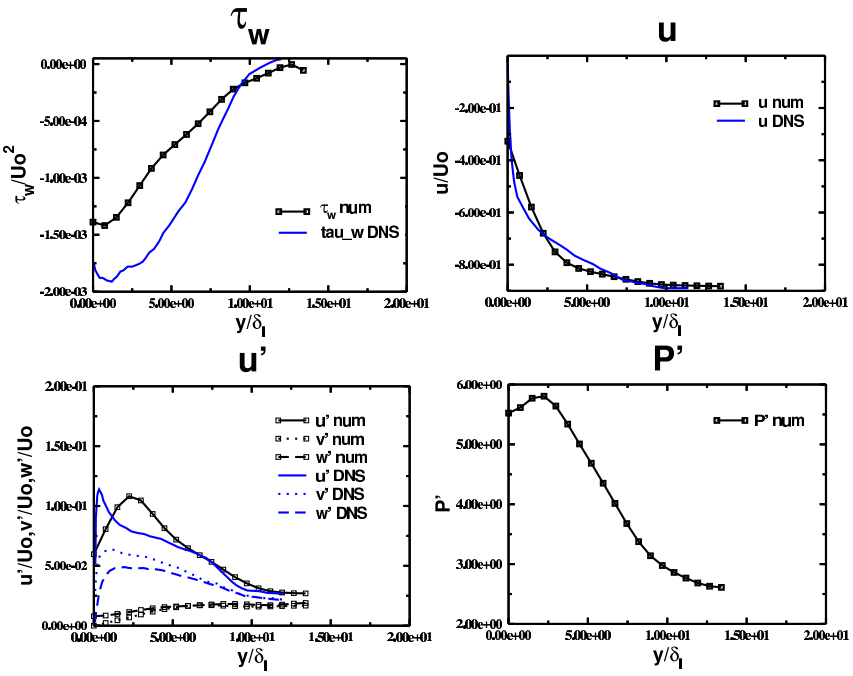


Figure 4: Phase $\pi/6$, Wall-Function Computation.

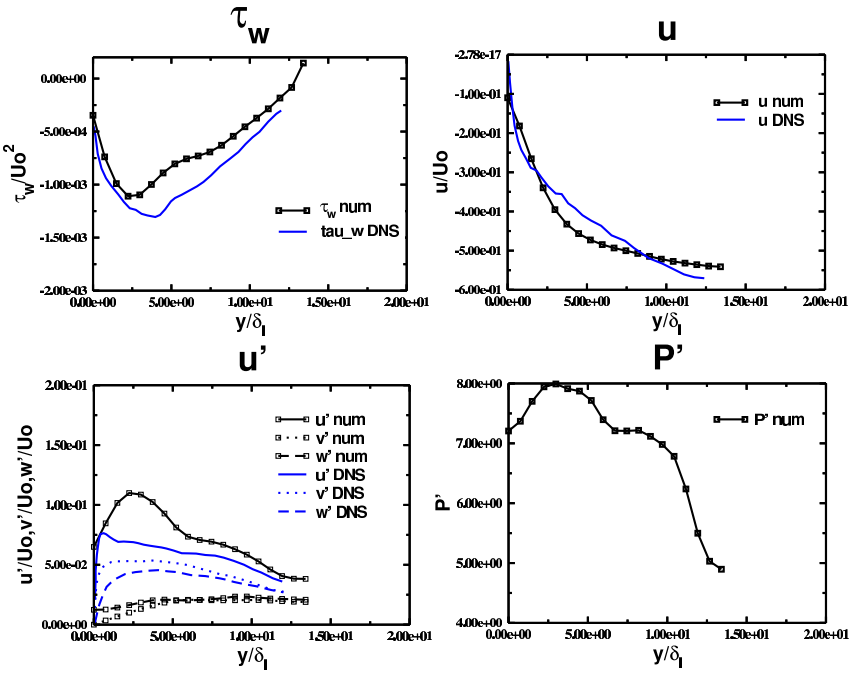


Figure 5: Phase $\pi/3$, Wall-Function Computation.

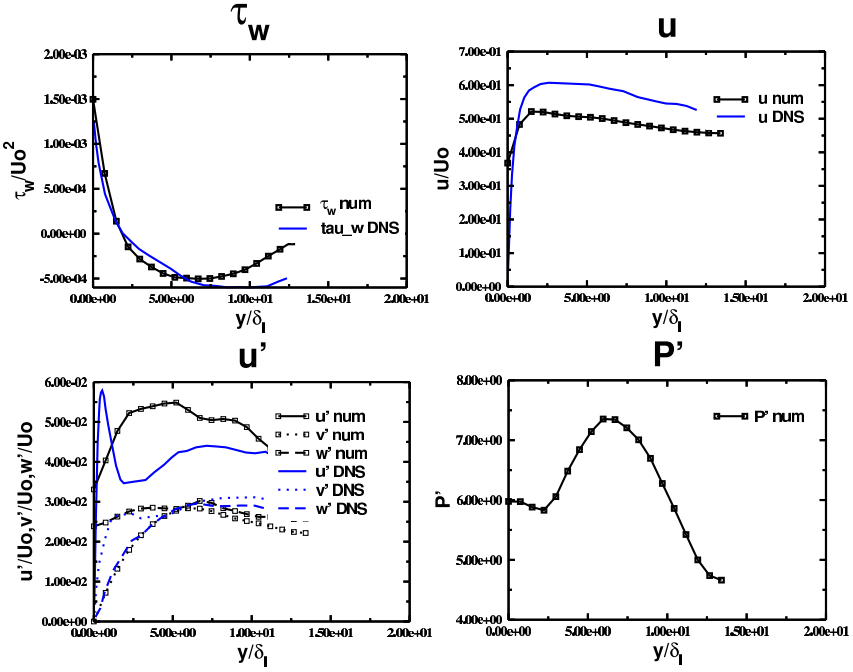


Figure 6: Phase $2\pi/3$, Wall-Function Computation.

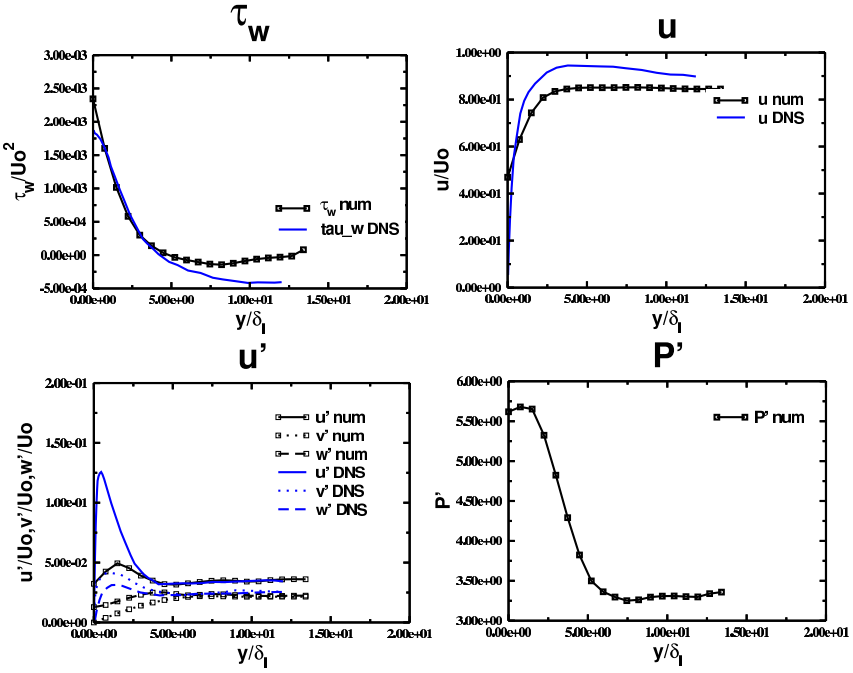


Figure 7: Phase $5\pi/6$, Wall-Function Computation.

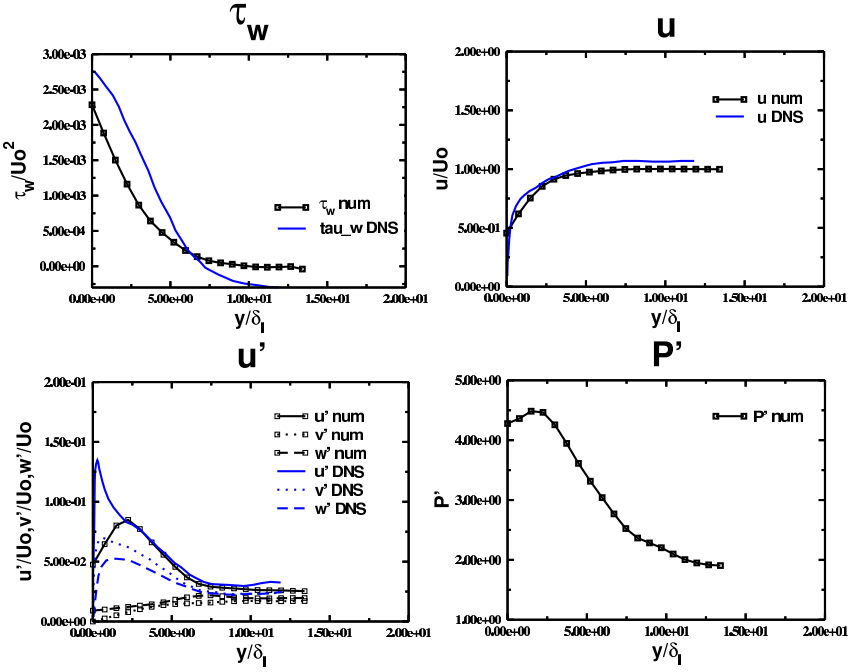


Figure 8: Phase $\pi$, Wall-Function Computation.

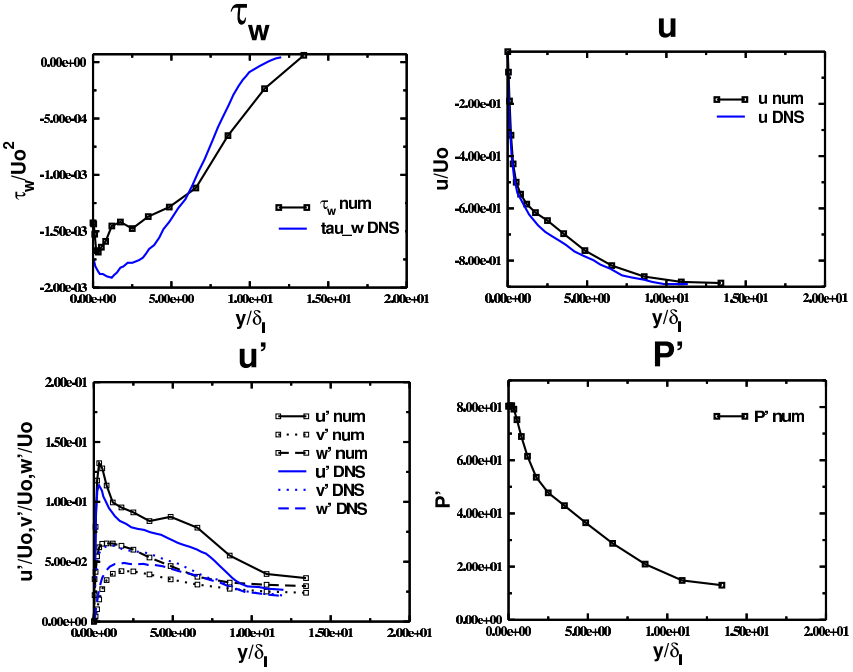


Figure 9: Phase $\pi/6$, Wall-Normal Resolved Computation.

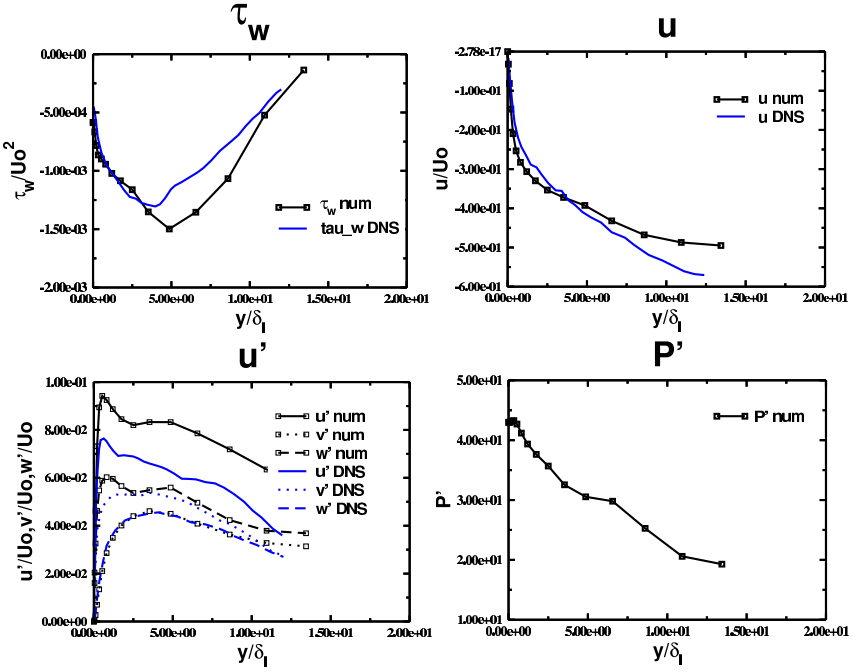


Figure 10: Phase $\pi/3$, Wall-Normal Resolved Computation.

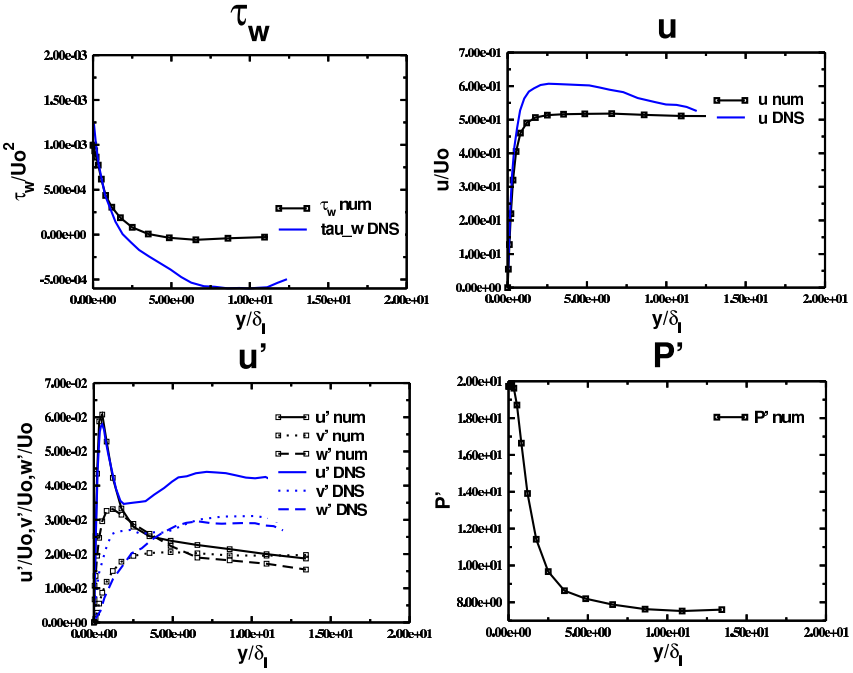


Figure 11: Phase $2\pi/3$, Wall-Normal Resolved Computation.

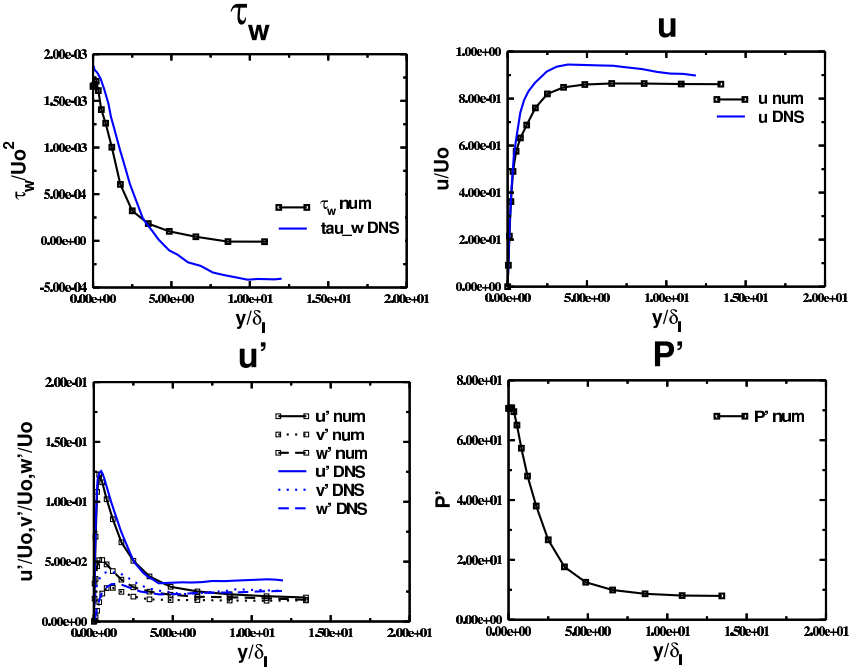


Figure 12: Phase $5\pi/6$, Wall-Normal Resolved Computation.

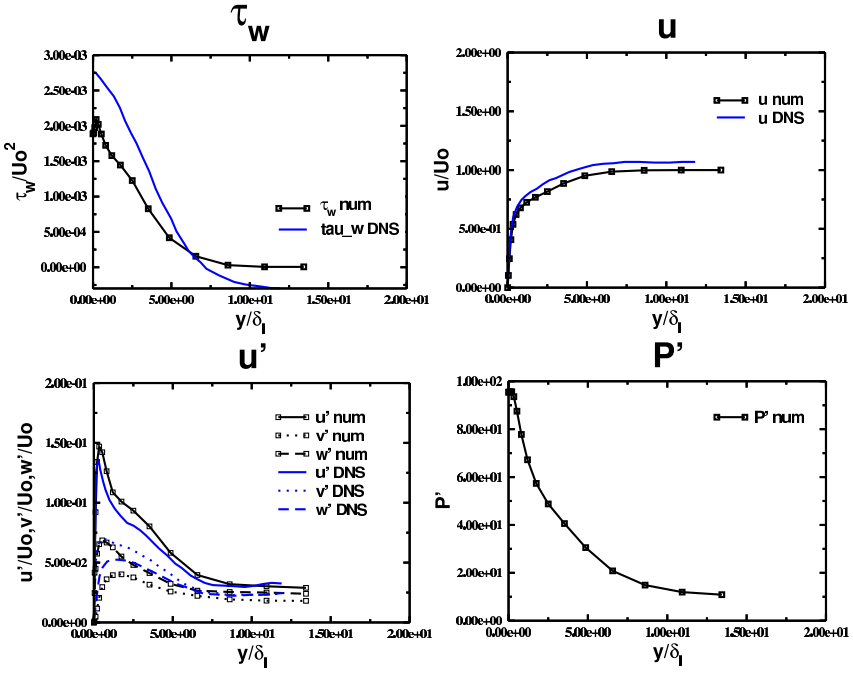


Figure 13: Phase $\pi$, Wall-Normal Resolved Computation.

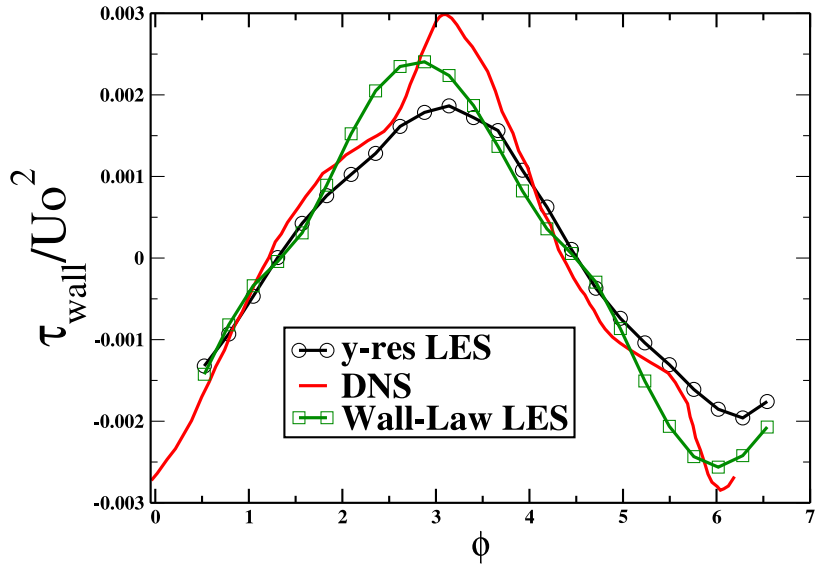


Figure 14: Wall-shear stress vs. phase, Wall-Normal Resolved and Wall Function Computation.

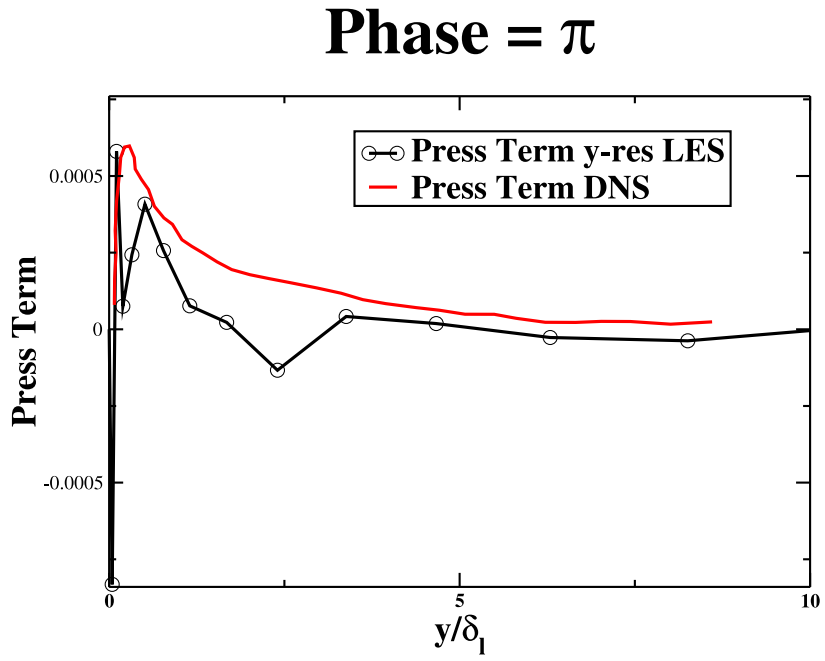


Figure 15: Pressure term, Reynolds stress budget.

## REFERENCES

[1] H. G. Weller, G. Tabor, H. Jasak and C. Fureby. A Tensorial Approach to Computational Continuum Mechanics using Object Orientated Techniques. *Computers in Physics*, **12-6**, 620–631, (1998)

[2] V. Moureau and G. Lartigue and Y. Sommerer and C. Angelberger and O. Colin and T. Poinsot. Numerical Methods for Unsteady Compressible Multi-Component Reacting Flows on Fixed and Moving Grids *Journal of Computational Physics*, **202-2**, 710–736, (2005).

[3] P. R. Spalart and B. S. Baldwin. Direct Simulation of a Turbulent Oscillating Boundary Layer. *Turbulent shear Flows* **6**, Springer-Verlag, (1989).

[4] S. F. Tardu and G. Binder and R. F. Blackwelder. Turbulent Channel Flow with Large-Amplitude Velocity Oscillations. *Journal of Fluid Mechanics*, **267**, 109–151, (1994).

[5] J. Smagorinsky. General Circulation Experiments with the Primitive Equations, I. The Basic Experiment. *Monthly Weather Review*, **91-3**, 99–164, (1963).

[6] F. Ducros, F. Nicoud and T. Poinsot. Wall-Adapting Local Eddy-Viscosity Models for Simulations in Complex Geometries. *ICFD*, 293–300, (1998).

[7] R. I. Issa. Solution of the Implicitly Discretised Fluid flow Equations by Operator-Splitting. *Journal of Computational physics*, **62**, 40–65, (1985).

[8] P. Scmitt. Simulation aux grandes échelles de la combustion étagée dans les turbines à gaz et son interaction stabilité - polluants-thermique - TH/CFD/05/45. *Institut National Polytechnique de Toulouse*. PhD Thesis, 2005.

[9] B. E. Launder and B. I. Sharma. Application of the Energy Dissipation Model of Turbulence to the Calculation of Flow Near a Spinning Disc. *Letters in Heat and Mass Transfer*, **1**, 131–138, (1974).